Ultrafast and Low Temperature Synthesis of Highly Crystalline and Patternable Few-Layers Tungsten Diselenide by Laser Irradiation Assisted Selenization Process

Yu-Ze Chen,[†] Henry Medina,[†] Teng-Yu Su,[†] Jian-Guang Li,[†] Kai-Yuan Cheng,[‡] Po-Wen Chiu,[‡] and Yu-Lun Chueh[*,†]

[†]Department of Materials Science and Engineering, National Tsing Hua University, Hsinchu 30013, Taiwan, ROC and [‡]Institute of Electronic Engineering, National Tsing Hua University, Hsinchu 30013, Taiwan

ABSTRACT Recently, a few attempts to synthesize monolayers of transition metal dichalcogenides (TMDs) using the chemical vapor deposition (CVD) process had been demonstrated. However, the development of alternative processes to synthesize TMDs is an important step because of the time-consuming, required transfer and low thermal efficiency of the CVD process. Here, we demonstrate a method to achieve few-layers WSe_2 on an insulator *via* laser irradiation assisted selenization (LIAS) process directly, for which the amorphous WO_3 film undergoes a reduction process in the presence of selenium gaseous vapors to form WSe_2, utilizing laser annealing as a heating source. Detailed growth parameters such as laser power and laser irradiation time were investigated. In addition, microstructures, optical and electrical properties were investigated. Furthermore, a patternable WSe_2 concept was demonstrated by patterning the WO_3 film followed by the laser irradiation. By combining the patternable process, the transfer-free WSe_2 back gate field effect transistor (FET) devices are realized on 300 nm-thick SiO_2/P^+Si substrate with extracted field effect mobility of $\sim$0.2 $cm^2\ V^{-1}\ s^{-1}$. Similarly, the reduction process by the laser irradiation can be also applied for the synthesis of other TMDs such as $MoSe_2$ from other metal oxides such as MO_3 film, suggesting that the process can be further extended to other TMDs. The method ensures one-step process to fabricate patternable TMDs, highlighting the uniqueness of the laser irradiation for the synthesis of different TMDs.

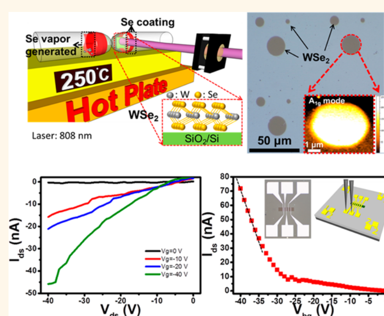

KEYWORDS: WO_3 · TMDs · laser irradiation assisted-selenization process · $MoSe_2$ · patternable growth

Recently, because of the layered structure with van der Waals forces between the layers similar to graphite, transition metal dichalcogenides (TMDs) have attracted significant attention.[1,2] Compared with the zero band gap feature in graphene, TMDs have their own band gap and are regarded as potential alternative materials to graphene for the next generation of opto- and nanoelectronics.[3,4] Recent research had pointed out that the electronic structure of TMDs has a layer-dependent relation. When the thickness of TMDs was reduced from bulk to monolayer, quantum confinement effect would alter the electronic structures in TMDs from indirect to direct bandgap and gives to rise the valley polarization, which in turn enhances the photoluminescence, making them highly competitive for optoelectronics applications.[3,5−8] Experimental results had revealed that exfoliated monolayer MoS_2 and WSe_2-based transistor show impressive carrier mobilities (200−500 $cm^2\ V^{-1}\ s^{-1}$) with high on/off ratio.[9,10] In addition, WSe_2 was found to have ambipolar behavior for potential use as p-type or n-type FET for COMS integration application.[10,11]

To date, the main obstacle in using TMDs into applications is development of the manufacturing process, which could lead to production of TMDs thin film with large area and high quality. Conventional top-down methods such as mechanical exfoliation,[1,2,9,12−14] lithium-based intercalation[15−17] and plasma-thinning process[18]

* Address correspondence to ylchueh@mx.nthu.edu.tw.

Received for review February 3, 2015 and accepted March 13, 2015.

Published online March 13, 2015
10.1021/acsnano.5b00866

© 2015 American Chemical Society

are time-consuming and low-yield processes, while the amount of layers of resulting TMDs are uncontrollable ranging from few micrometer to few nanometer (few-layers). The TMD flakes prepared by ion intercalation method would suffer from contamination, degrading the electrical properties. On the contrary, the bottom-up synthesis of TMDs had been proposed, such as the thermolysis for growth of WSe_2,[19]direct deposition of MoS_2 by pulsed laser deposition (PLD) process.[20] However, the requirement of high temperature for thermolysis of WSe_2 and the dependence on expensive PLD systems would hinder its real popularization and mass production in industry.

Recently, sulfurization or selenization of transition metal oxides through chemical vapor deposition (CVD) process successfully enables monolayer TMDs in large-area with high quality.[21−23] However, the CVD process requires high temperature annealing processes (627−1300 °C) and belongs to time-consuming process, which limits the substrates used for synthesis of TMDs while the additional transfer process of TMDs is still required. Hence, the development of ultrafast and low cost synthesis method remains as a major challenge. In this regard, we demonstrate an ultrafast (<20 min) and low-cost approach to synthesize few-layers WSe_2 from the direct transformation of WO_3 to WSe_2 by the laser irradiation assisted-selenization (LIAS) process. Microstructures, optical and electrical properties were investigated in detail. Growth parameters such as laser power and laser irradiation time were investigated. The detailed transformation mechanisms from the transition metal oxide into TMDs triggered by laser was discussed and investigated as well. Furthermore, patternable WSe_2 concept was demonstrated by direct patterning the WO_3 film followed by the laser irradiation process. Similarly, the reduction process by the laser irradiation can be also applied for the synthesis of other TMDs from other metal oxide such as $MoSe_2$ from MO_3 films, suggesting that the process can be further extended to other TMD materials.

RESULTS AND DISCUSSION

Figure 1(a) shows the schematic illustration of the concept how we performance the rapid synthesis of the WSe_2 by the LIAS process. A WO_3 film with controllable thicknesses (2 nm in our case) was directly deposited on a 300 nm-thick SiO_2/Si substrate by electron beam evaporation and was placed in a vacuum-sealed quartz tube with 0.1 g of Se ingots at 10^{-4} Torr (Figure 1a). In order to prevent the contamination from melting of Se ingots when rolling and touching the samples, a neck on the quartz tube was intentionally created to isolate the WO_3/SiO_2/Si substrate and the Se ingots, only allowing the transport of Se vapors through the neck area during the heating process as shown in Figure S1a (Supporting Information). Because of the low melting point of Se

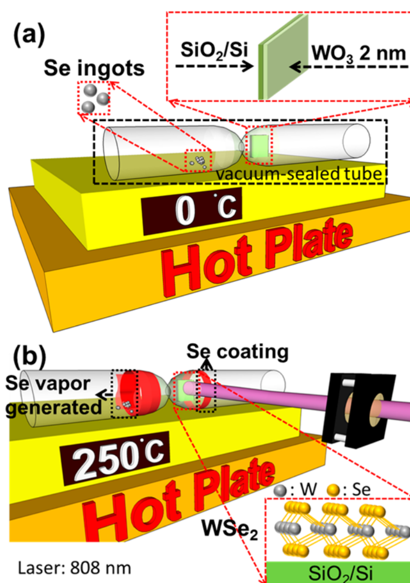

Figure 1. A schematic of few-layers WSe_2 growth by the laser irradiation process. (a) 2 nm-thick WO_3 on SiO_2/Si and Se ingots was vacuum-sealed together. (b) When quartz tube heated up to 250 °C by hot plate, Se vapor was generated and flowed to WO_3 irradiated by laser, resulting information on WSe_2.

(220.8 °C), the generation of Se vapors can be achieved at the relatively low temperature. For synthesis of highly crystalline few-layers WSe_2 as shown in Figure 1(b), the vacuum-sealed quartz tube was placed on a hot plate with an annealing temperature of 250 °C for a few minutes in order to allow the Se vapor to be homogeneously distributed along the quartz tube. Then, a continuous wave laser with wavelength of 808 nm was utilized to trigger the substrate heating. While the laser is locally irradiated on the samples as shown in Figure S1b, the WO_3 is heated and reduced with Se vapors generated by hot plate in the vacuum-sealed quartz tube. As a result, few-layers WSe_2 on 300 nm SiO_2/Si substrate can be synthesized (Figure 1b) *via* the following chemical reaction:

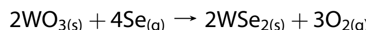

$$2WO_{3(s)} + 4Se_{(g)} \rightarrow 2WSe_{2(s)} + 3O_{2(g)}$$

Figure 2(a) shows optical images of the deposition of the WO_3 film before and after the laser irradiation process. The deposition of 2 nm-thick WO_3 on the SiO_2/Si substrate has a distinct contrast between the interface of WO_3 and SiO_2. After the synthesis of the WSe_2 by the laser irradiation process, it is easily observed by naked eye the change of the color from light green to dark blue (Figure 2a). Furthermore, Raman spectrum excited by 632.8 nm laser was used to confirm the phase changes from WO_3 to WSe_2 taken from the area (b1) in Figure 2(a) after the laser irradiation as shown in Figure 2(b1). In addition, the Raman spectrum of the as-deposited WO_3 film on the SiO_2/Si substrate was measured as reference. Note that the

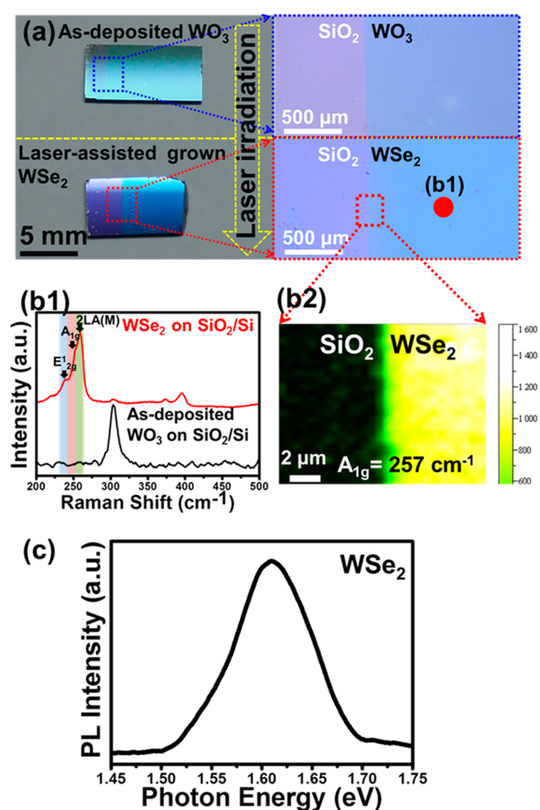

Figure 2. (a) The OM images of as-deposited WO_3 and laser-induced WSe_2 on the SiO_2/Si substrate, respectively. (b) Its characteristic Raman spectrum and corresponding Raman mapping for WSe_2 at A_{1g} = 251 cm^{-1} mode and (c) photoluminescence spectra of WSe_2 after the laser irradiation process.

peak at 300 cm^{-1}, corresponding to one of the characteristic vibrational modes of intrinsic Si, was measured because the WO_3 Raman peak cannot be observed probably due to the amorphous nature of the WO_3 deposited by electron-beam evaporation (Figure S2). However, after the laser irradiation process, three distinctive bands located at 245, 251 and 257 cm^{-1} corresponding to the characteristic E^1_{2g}, A_{1g} and 2LA(M) bands of WSe_2 due to the out-of-plane, in-plane vibrational modes and second-order Raman scattering of the LA phonon were measured, distinctly indicating the successful reduction of WSe_2 from WO_3.[13,14,24] To further characterize the uniformity of the obtained WSe_2 film, Raman mapping image at A_{1g} of ~251 cm^{-1} mode excited by the 632.8 nm laser with a scanning area 20 × 20 μm^2 was acquired as shown in Figure 2(b2). Obviously, the uniform contrast indicates the uniform reduction of the WSe_2 from the WO_3. Furthermore, the photoluminescence (PL) spectrum of the synthesized WSe_2 excited by 632 nm laser (Figure 2c) exhibits a strong phonon emission at around 1.65 eV, which is in perfect agreement with previous works, confirming the growth of the few-layers WSe_2.[13,24]

High-resolution transmission electron microscopy (HR-TEM) was utilized to reveal the characteristic layered structure of the WSe_2. Prior to the cross-sectional TEM observation, TEM sample was prepared by focused ion beam (FIB). In order to avoid the damage caused by Ga ion bombardment during the FIB process, a 100 nm-thick SiO_2 layer was deposited on the WSe_2. Figure 3(a) shows a typical cross-sectional bright-field TEM image. Obviously, the thickness of synthesized WSe_2 is around 2 nm, which corresponds to 3–4 atomic WSe_2 layers. Notably, the magnified cross-sectional TEM image shows the characteristic layer structure with interspacing of 0.69 nm as shown in Figure 3(b), which is in excellent agreement with the interlayer distance of exfoliated WSe_2 from previous report.[13] Furthermore, the compositional analysis of the few-layers WSe_2 was also measured by energy dispersive X-ray spectroscopy (STEM-EDX) as summarized in Table 1. Obviously, elemental compositions of ~39.53 and ~60.47 at. % for Se and W were measured, showing that the W/Se ratio is close to 0.5 and confirming the good stoichiometry of the synthesized few-layers WSe_2. Most importantly, the TEM image indeed shows the controlled number of WSe_2 atomic layers by the controlled WO_3 thickness deposition.

To further understand the reduction mechanism from WO_3 to WSe_2 influenced by different laser powers, the evolution of growth for few-layers WSe_2 from WO_3 at different laser power was examined by Raman spectra, as illustrated in Figure 4(a) while keeping the laser irradiation time at 20 min. As a laser power of 5.79 W was applied, a broaden peak at ~250 cm^{-1} can be observed, which is close to the expected position of the WSe_2 A_{1g} band while no 2LA (M) can be differentiated (Figure 4a1). It is more likely that the observed peak

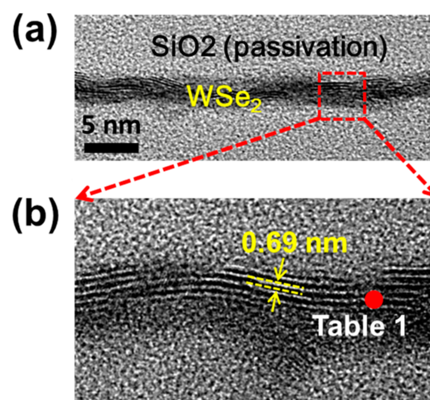

Figure 3. (a) A cross-sectional TEM image of WSe_2, and (b) a higher magnification of TEM image, which reveals the typical interlayer distance of the WSe_2.

TABLE 1. Compositional Results Taken an Region As Shown in Figure 3(b)

element	atomic %
Se K	39.53
W L	60.47
total	100.00

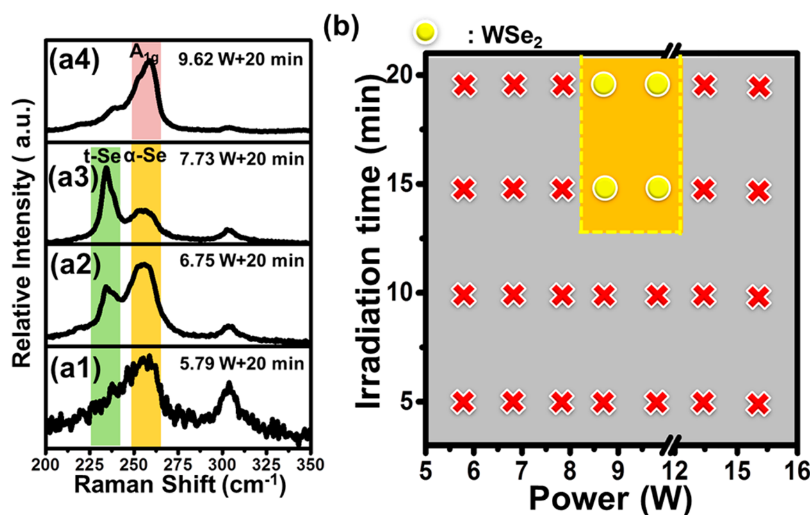

Figure 4. (a) Raman spectra of WO_3 to WSe_2 with varied laser powers and irradiation time. (b) The growth window for the reduction of WO_3 film to few-layers WSe_2 at different laser powers and irradiation time.

corresponds to amorphous selenium (a-Se) rather than WSe_2, indicating lack of crystallinity.[25] Because of the low melting point of Se, Se powers are easily vaporized. If the laser power and time illuminated on the substrate are insufficient to trigger the selenization of the WO_3 film, Se vapor would be merely condensed on the WO_3 film, resulting in the deposition of a-Se. In addition, the additional peak at 300 cm^{-1} is contributed from the SiO_2/Si substrate as shown in Figure S2. By gradually increasing the laser power to 6.75 and 7.73 W at the fixed irradiation time of 20 min, an additional peak located at ~237 cm^{-1} was measured (Figures 4a2 and 4a3). Masuzawa *et al.*[26] point out that α-Se undergoes a crystallization process into crystalline t-Se (237 cm^{-1}) at an elevated temperature. Therefore, it is reasonable to believe that α-Se would experience a crystallization transformation from amorphous to crystalline t-Se due to the increased temperature during the laser irradiation process in our case. However, the presence of α-Se and t-Se peaks indicates that the energy gained from the laser irradiation is insufficient to trigger the chemical reduction process between Se and WO_3. Thus, by further increasing the laser power to ~9.62 W, the characteristics of A_{1g} and 2LA(M) bands of the WSe_2 appear, indicating a noticeable transformation happened from WO_3 into WSe_2 (Figure 4a4). Furthermore, we found that the irradiation time also plays a key role in the reduction process. Even at a laser power over 9.62 W, the Raman signal of WSe_2 is not strong enough, suggesting the poor crystallinity of the few-layers WSe_2 due to noncomplete reduction process when the irradiation time is under 15 min while the characteristic Raman spectra of WSe_2 shows a strong intensity, suggesting a good crystallinity of the few-layers WSe_2 once the irradiation time is over 15 min. Figure 4 (b) shows the summarized parameters in the growth window of WSe_2 *via* the laser irradiation. Note that the growth condition of the few-layers WSe_2 by the laser irradiation is quite narrow. If the power of the laser is below 8 W, only t-Se and a-Se are obtained. However, for laser power over ~13 W, no Raman signal of the WSe_2 can be detected, which is expected due to evaporation of WO_3 film during the laser irradiation process. As a result, according to experimental results, setting the power of the laser at ~8−10 W for 20 min irradiation time was the best condition for the growth of few-layers WSe_2 in our current study while it may be changed due to different laser and annealing environments. Importantly, we found that the sample position relative to the laser is also a critical factor to achieve good quality of the few-layers WSe_2. Note that our laser system uses a confocal lens with a focal length of 7 cm (Figure S3a). By placing samples at the focus point, a spot with a diameter of 300 μm was found at the surface of samples while no characteristic peaks of the few-layers WSe_2 examined by Raman spectrometer were found after the laser power and irradiation time of 9 W and 20 min, respectively. The disappearance of Raman spectra are mostly like due to thermal damage by the laser irradiation process as shown in Figure S3b. To avoid the damage caused by the laser irradiation process, the sample was placed out of focus at 10 cm to diverge the exposed total area of the sample, giving rise to uniform few-layers WSe_2 as shown in Figure S3b. In addition, the curvature of quartz tube is another reason to slightly diverge the laser beam, increasing the difficulty to estimate the adsorbed power by the substrate.

In order to obtain the bonding information on the few-layers WSe_2, X-ray photoemission spectroscopy (XPS) was conducted to acquire the binding energies of W 1s and Se 1s, respectively. Figure 5(a) displays the corresponding W 1s spectra before and after the laser irradiation process. For the pristine WO_3 film, the peaks located at 37 and 39 eV are the footprints of W $4f_{7/2}$ and W $4f_{5/2}$.[27] After the reduction of the WO_3 into the

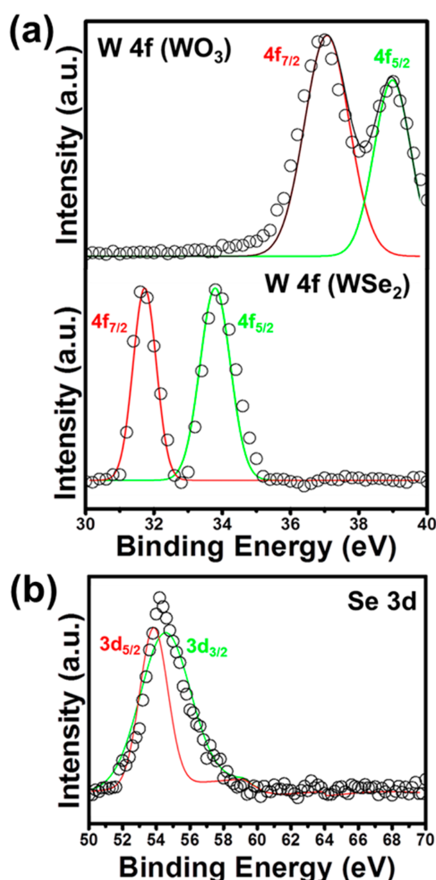

Figure 5. (a) XPS spectroscopy of the W 1s spectra before and after the laser irradiation, and (b) the Se 1s spectra after the irradiation.

few-layers WSe_2, W $4f_{7/2}$ and W $4f_{5/2}$ peaks, suffering a chemical shift to 31.8 and 33.8 eV, respectively. This large down-shift perfectly agrees with the expected W $4f_{7/2}$ and W $4f_{5/2}$ band position of WSe_2 attributed to the low electronegativity of Se compared with O.[28] In addition, the Se 1s spectra shown in Figure 5(b) distinctly reveal two new peaks located at 54 and 55 eV, which are also consistent with Se $3d_{5/2}$ and Se $3d_{3/2}$ peaks of the few-layers WSe_2.[28] The above results were consistent with previous research,[29] which implied the highly crystalline WSe_2 we successfully obtained.

Contrary to the CVD process, the laser irradiation process is an ultrafast process compared to the typical CVD process, which needs at least 80 min per run, including preheating and cooling processes while requiring to heat up the whole chamber with temperature more than 1000 °C.[21−23] The current approach could achieve the formation of WSe_2 within 20 min and only the local heating of the Se precursors are required, indicating a rapid and low-thermal budget process. In addition, the thickness of the grown WSe_2 is controllable, depending on the initial thickness of the WO_3 film. Because of the limit of thickness control by electron beam evaporation, the thinnest uniform thickness of the WO_3 in our study is around ∼2 nm, yielding few-layers WSe_2 after the laser irradiation process.

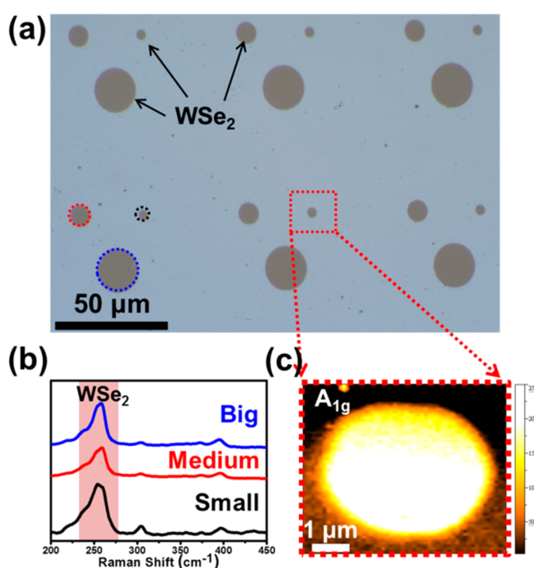

Figure 6. (a) An optical image of the prepatterned few-layers WSe_2 after the irradiation process. (b) The typical Raman spectra at the three different regions marked in (a). (c) A Raman mapping image of the A_{1g} mode for prepatterned few-layers WSe_2 at the patterned region in (a).

TABLE 2. Comparison Table for the Growth of TMDs with Different Growth Methods

methods	process and comparison
exfoliation by Scotch tape[1,2,9,12−14]	time-consuming, low yield, high quality
lithium-based intercalation[15−17]	purification needed, restacked
vapor−solid growth[19]	high temperature, lack of electrical performance
pulsed laser deposition[20]	expensive facility, transfer process needed
chemical vapor deposition[21−23]	time-consuming, scalable
plasma-induced thinning[18]	time-consuming, patternable
laser irradiation	quick, patternable

However, we believe that monolayer WSe_2 is achievable as long as we can deposit very thin and uniform WO_3 by other methods such as atomic layer deposition,[30] molecular beam epitaxy[31] and pulsed laser deposition.[32] Furthermore, the current approach allows the pattern-ability on the WSe_2. By using standard lithography methods, WO_3 patterns can be created, followed by the laser irradiation process. Figure 6(a) displays the optical image of the patterned few-layers WSe_2 obtained after the laser irradiation from the prepatterned WO_3 film in circular shape by optical lithography. The Raman spectra presented in Figure 6(b) and the corresponding Raman mapping images at A1g in Figure 6(c) confirm the successful transformation of the patterned few-layers WSe_2 from the prepatterned WO_3 film. We expect that the prepattern process of the WO3 film to directly achieve the patterned WSe_2 can further reduce the complexity of the device fabrication. To shed light on the growth of the

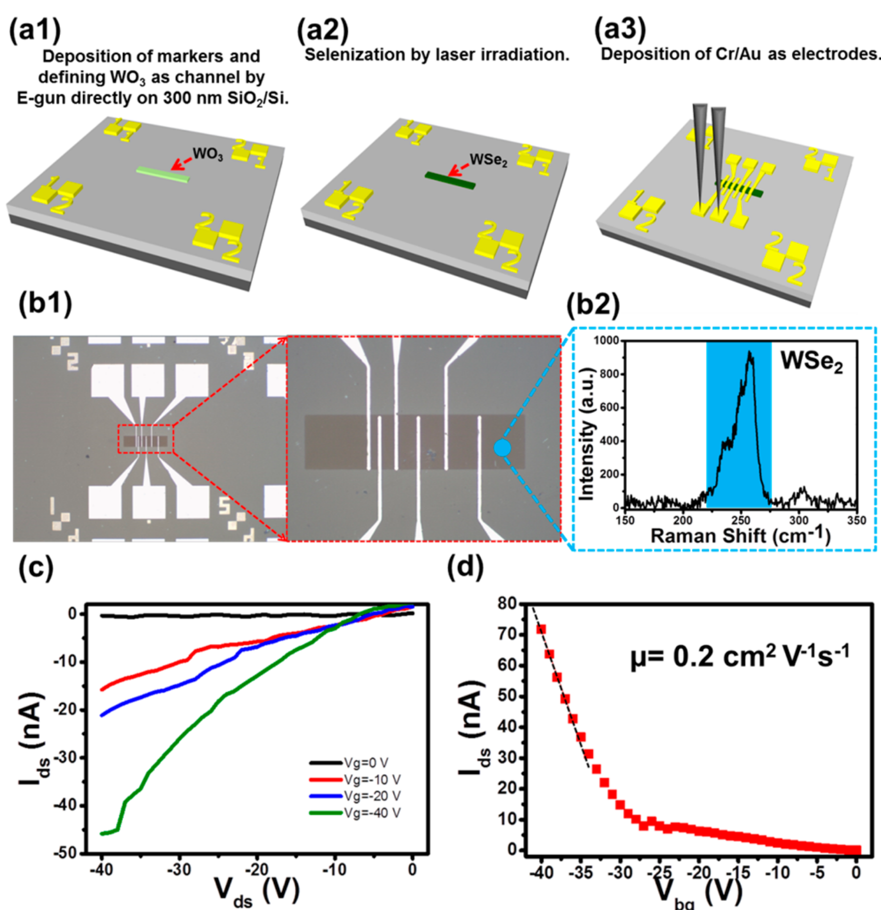

Figure 7. (a1−a3) Schematics of fabrication process of WSe_2 FET devices. An optical image of the prepatterned few-layers WSe_2 after the irradiation process. (b1) Optical images of WSe_2−FET devices and (b2) the corresponding Raman spectrum at the channel marked in (b1). (c) I_{ds}−V_{ds} characteristics of back gate WSe_2 FET devices at different back gate biases with 5 nm Cr and 50 nm Au as the electrode. (d) I_{ds}−V_{bg} characteristics of the back gate WSe_2 FET devices at $V_{ds} = -10$ V in hole-conduction channel.

TMD by the laser irradiation process, different growth methods of the TMDs and uniqueness of each growth method was listed in Table 2. Quick and direct patternable growth are promising properties of the laser irradiation process. In addition, laser-assisted selenization process was enabled to simplify the fabrication process of FET devices and free of chemical etchant.

To demonstrate and evaluate the electrical performance of few-layers TMDs by combining the direct patternable growth, the schematics of the transfer-free WSe_2 back gate field effect transistor (FET) devices are shown in Figure 7(a1−a3), with which the thickness of 300 nm SiO_2 layer was used as the dielectric layer on P^+-Si substrate. First, the prepatterned WO_3 was deposited as the channel (Figure 7a1). After the selenization by the laser irradiation and deposition of Cr/Au metal as electrodes (Figure 7a2−a3), the few-layers WSe_2 FET devices can be finally fabricated. The corresponding real optical images of the few-layers WSe_2−FET device is shown in Figure 7(b1) and the Raman spectrum as shown in Figure 7(b2) distinctly confirms the direct formation of the few-layers WSe_2 as the channel materials. The I_{ds}−V_{ds} characteristics at different V_{bg} biases were measured in the hole-conduction channel, as shown in Figure 7(c). Clearly, the enhanced conductance can be found once the back gate bias increases, indicating the P-type semiconductor, which is consistent with the report from the literature.[23] I_{ds}−V_{bg} at $V_{ds} = 10$ V is shown in Figure 7(d), indicating an on/off ratio > ∼70. In addition, the field effect mobility of ∼0.2 $cm^2\ V^{-1}\ s^{-1}$ was calculated based on the equation $\mu = (L/WC_{ox}V_{ds})(\Delta I_{ds}/\Delta V_{bg})$ at the linear region of $\Delta I_{ds}/\Delta V_{bg}$ where L and W are defined as channel length and width, respectively and C_{ox} is the gate capacitance (300 nm-thick SiO_2). Although, the field effect mobility of the few-layers WSe_2 is low, the result is still comparable with previous studies of WSe_2 prepared by mechanical exfoliation[12] and CVD growth approaches.[23] The low mobility is most likely the oxygen content in the film.[23] Because of the nature of our process, it is likely to have residual WO_3 remaining inside the film, which may influence the electrical performance. Furthermore, the polycrystalline WSe_2 with limited domain size after the laser irradiation assisted-selenization process on the amorphous as-deposited WO_3 film may also result in

degrading the electrical performance because of phonon−electron scattering. As a result, we believe that the improved electrical performance of WSe_2 film can be achieved once the uniformity and quality of WO_3 is improved.

Importantly, the laser irradiation process can be further extended to other TMDs. Similar to WSe_2, the growth of the few-layers $MoSe_2$ on the SiO_2/Si substrate can be also demonstrated by the laser irradiation process using the MoO_3 film instead of the WO_3 film (Figure S4). Figure S4(a) shows the characteristic Raman spectrum after transforming the 2 nm-thick MoO_3 into the few-layers $MoSe_2$. Obviously, two characteristic peaks located at 240 and 283 cm^{-1} are assigned to A_{1g} and $E^1{}_{2g}$, which matches with that of exfoliated[13,14] and CVD-grown $MoSe_2$.[33] In addition, the Raman mapping of the $MoSe_2$ A_{1g} band displayed in Figure S4(c) shows high uniformity in large scale. Furthermore, the photoluminescence (PL) spectrum (excited by 632 nm laser) of the synthesized $MoSe_2$ exhibited a strong emission of photons at around 1.55 eV. It is noteworthy to mention that previous works suggest the necessity of the introduction of hydrogen to trigger the transformation of WO_3 to WSe_2 during the selenization process.[21−23] In our experimental setup, the quartz tube including WO_3 and Se ingots inside was sealed in a vacuum of 10^{-4} Torr without introducing any gases, such as hydrogen and WSe_2 was also successfully synthesized by the laser irradiation in the vacuum-sealed quartz tube. We suggest that the higher vacuum level in our experiment could provide a suitable environment for the synthesis of TMDs.[21,34]

CONCLUSIONS

WSe_2 have been successfully synthesized by the laser irradiation process. Contrary to the long and energy-wasting CVD process, the laser approach is able to achieve an ultrafast heating process, leading to the growth of few-layers WSe_2 in short time. Because of the local heating induced by the laser directly exposed to the WO_3, the process is highly thermal-energy efficient. Detailed and systematic investigation was provided by Raman analysis, XPS analysis and TEM observations. Furthermore, patternable WSe_2 concept was demonstrated by directly patterning the WO_3 film followed by the laser irradiation process. By combining the patternable process, the transfer-free WSe_2 back gate field effect transistor (FET) devices are realized using the 300 nm SiO_2/P^+Si substrate. The field effect mobility of ∼0.2 $cm^2\ V^{-1}\ s^{-1}$ can be extracted. Similarly, the reduction process by the laser irradiation can be also applied for the synthesis of other TMDs from other metal oxides such as $MoSe_2$ from MO_3 films, suggesting that the process can be further extended to other TMDs.

METHODS

Sample Preparation and Laser-Irradiation. First, 2 nm-thick WO_3 was deposited on thermally oxidized 50/300 nm SiO_2/Si by electron beam evaporation. Second, WO_3/SiO_2/Si and Se ingots were placed into 0.5 in. quartz tube and vacuumed to a 10−4 Torr for a while. Then, quartz tube was sealed by oxy-propane flame. A continuous wave 808 nm laser was used as the main heating source to the substrate, while Se vapor was generated Se using a hot plate set at 250 °C (Coring PC-420). Once the laser irradiation was finished, the quartz tube was removed from the hot plate and rapid cooled by air.

Characterizations. Morphologies, lattice spacing and elemental compositions were acquired by high resolution transmission electron microscopy (HRTEM, JEOL, JEM-3000F FEGTEM, 300 kV) equipped with Energy Dispersive Spectroscopy (EDS by INCA analysis system, Oxford Instruments). Micro-Raman spectroscopy (HORIBA, LabRAM, HR800) equipped with a 632.8 nm laser was used to examine the quality and uniformity of WSe_2. The photoluminescence (PL) spectrum was acquired using the same system. X-ray photoemission spectroscopy equipped with a monochromatic Al Kα X-ray source (XPS, Ulvac-PHI 1600) was carried out to obtain the bonding information.

Conflict of Interest: The authors declare no competing financial interest.

Acknowledgment. The research is supported by Ministry of Science and Technology through Grants No. 101-2112-M-007-015-MY3, 101-2218-E-007-009-MY3, 103-2633-M-007-001, and the National Tsing Hua University through Grant No. 104N2022E1. Y. L. Chueh greatly appreciates the use of facility at CNMM, National Tsing Hua University through Grant No. 104N2744E1.

Supporting Information Available: Experimental Methods; pictures of quartz tube including Se ingots and WO_3/SiO_2/Si and experiment setup during the laser irradiation; pictures of quartz tube irradiated by laser at the focus point and at the out of focus point and its corresponding OM image after the laser irradiation process, respectively; Raman spectrum of Si, 50 nm-thick SiO_2/Si, 2 nm-thick WO_3/SiO_2/Si; Raman spectrum and mapping of $MoSe_2$ and PL spectrum of $MoSe_2$. This material is available free of charge *via* the Internet at http://pubs.acs.org.

REFERENCES AND NOTES

1. Novoselov, K. S.; Jiang, D.; Schedin, F.; Booth, T. J.; Khotkevich, V. V.; Morozov, S. V.; Geim, A. K. Two-Dimensional Atomic Crystals. *Proc. Natl. Acad. Sci. U. S. A.* **2005**, *102*, 10451–10453.
2. Mak, K. F.; Lee, C.; Hone, J.; Shan, J.; Heinz, T. F. Atomically Thin MoS_2: A New Direct-Gap Semiconductor. *Phys. Rev. Lett.* **2010**, 105.
3. Kumar, A.; Ahluwalia, P. K. Electronic Structure of Transition Metal Dichalcogenides Monolayers 1H-MX_2 (M = Mo, W; X = S, Se, Te) from *Ab-Initio* Theory: New Direct Band Gap Semiconductors. *Eur. Phys. J. B* **2012**, 85.
4. Kuc, A.; Zibouche, N.; Heine, T. Influence of Quantum Confinement on the Electronic Structure of the Transition Metal Sulfide TS_2. *Phys. Rev. B: Condens. Matter Mater. Phys.* **2011**, *83*, 245213.
5. Splendiani, A.; Sun, L.; Zhang, Y.; Li, T.; Kim, J.; Chim, C. Y.; Galli, G.; Wang, F. Emerging Photoluminescence in Monolayer. *Nano Lett.* **2010**, *10*, 1271–1275.
6. Korn, T.; Heydrich, S.; Hirmer, M.; Schumutzler, J.; Schuller, C. Low-Temperature Photocarrier Dynamics in Monolayer MoS_2. *Appl. Phys. Lett.* **2011**, 99.
7. Molina-Sanchez, A.; Wirtz, L. Phonons in Single-Layer and Few-Layer MoS_2 and WS_2. *Phys. Rev. B: Condens. Matter Mater. Phys.* **2011**, 84.

8. Cheng, R.; Li, D.; Zhou, H.; Wang, C.; Yin, A.; Jiang, S.; Liu, Y.; Chen, Y.; Huang, Y.; Duan, X. Electroluminescence and Photocurrent Generation from Atomically Sharp WSe_2/MoS_2 Heterojunction p−n Diodes. *Nano Lett.* **2014**, *14*, 5590–5597.
9. Radisavljevic, B.; Radenovic, A.; Brivio, J.; Giacometti, V.; Kis, A. Single-Layer MoS_2 Transistors. *Nat. Nanotechnol.* **2011**, *6*, 147–150.
10. Fang, H.; Chuang, S.; Chang, T. C.; Takei, K.; Takahashi, T.; Javey, A. High-Performance Single Layered WSe_2 p-FETs Chemically Doped Contacts. *Nano Lett.* **2012**, *12*, 3788–3792.
11. Liu, W.; Kang, J.; Sarkar, D.; Khatami, Y.; Jena, D.; Banerjee, K. Role of Metal Contacts in Designing High-Performance Monolayer n-Type WSe_2 Field Effect Transistors. *Nano Lett.* **2013**, *13*, 1983–1990.
12. Li, H.; Lu, G.; Wang, Y.; Yin, Z.; Cong, C.; He, Q.; Wang, L.; Ding, F.; Yu, T.; Zhang, H. Mechanical Exfoliation and Characterization of Single and Few-Layer Nanosheets of WSe_2, TaS_2, and $TaSe_2$. *Small* **2013**, *9*, 1974–1981.
13. Terrones, H.; Del Corro, E.; Feng, S.; Poumirol, J. M.; Rhodes, D.; Smirnov, D.; Pradhan, N. R.; Lin, Z.; Nguyen, M. A. T.; Elias, A. L.; *et al.* New First Order Raman-Active Modes in Few Layered Transition Metal Dichalcogenides. *Sci. Rep.* **2014**, 4.
14. Tongay, S.; Suh, J.; Ataca, C.; Fan, W.; Luce, A.; Kang, J. S.; Liu, J.; Ko, C.; Raghunathanan, R.; Zhou, J.; *et al.* Defects Activated Photoluminescence in Two-Dimensional Semiconductors: Interplay between Bound, Charged, and Free Excitons. *Sci. Rep.* **2013**, 3.
15. Whittingham, M. S.; R. Gamble, F., Jr. The Lithium Intercalates of the Transition Metal Dichalcogenides. *Mater. Res. Bull.* **1975**, *10*, 363–370.
16. Joensen, P.; Frindt, R. F.; Morrison, S. R. Single-Layer MoS_2. *Mater. Res. Bull.* **1986**, *21*, 457–461.
17. Schumacher, A.; Scandella, L.; Kruse, N.; Prins, R. Single-Layer MoS_2 on Mica: Studies by Means of Scanning Force Microscopy. *Surf. Sci. Lett.* **1993**, 289.
18. Liu, Y.; Nan, H.; Wu, X.; Pan, W.; Wang, W.; Zhao, W.; Sun, L.; Wang, X.; Ni, Z. Layer-by-Layer Thinning of MoS_2 by Plasma. *ACS Nano* **2013**, *7*, 4202–4209.
19. Xu, K.; Wang, Z.; Du, X.; Safdar, M.; Jiang, C.; He, J. Atomic-Layer Triangular WSe_2 Sheets: Synthesis and Layer-Dependent Photoluminescence Property. *Nanotechnology* **2013**, 24.
20. Loh, T. A. J.; Chua, D. H. C. Growth Mechanism of Pulsed Laser Fabricated Few-Layer MoS_2 on Metal Substrates. *ACS Appl. Mater. Interfaces* **2014**, *6*, 15966–15971.
21. Huang, J.-K.; Pu, J.; Hsu, C.-L.; Chiu, M.-H.; Jaung, Z.-Y.; Chang, Y.-H.; Chang, W.-H.; Iwasa, Y.; Takenobu, T.; Li, L.-J. Large-Area Synthesis of Highly Crystalline WSe_2 Monolayers and Device Applications. *ACS Nano* **2014**, *8*, 923–930.
22. Lee, Y.-H.; Zhang, X.-Q.; Zhang, W.; Chang, M.-T.; Lin, C.-T.; Chang, K.-D.; Yu, Y.-C.; Wang, J. T.-W.; Chang, C.-S.; Li, L.-J.; *et al.* Synthesis of Large-Area MoS_2 Atomic Layers with Chemical Vapor Deposition. *Adv. Mater.* **2012**, *24*, 2320–2325.
23. Liu, K.-K.; Zhang, W.; Lee, Y.-H.; Lin, Y.-C.; Chang, M.-T.; Su, C.-Y.; Chang, C.-S.; Li, H.; Shi, Y.; Zhang, H.; *et al.* Growth of Large-Area and Highly Crystalline MoS_2 Thin Layers on Insulating Substrates. *Nano Lett.* **2012**, *12*, 1538–1544.
24. Zhao, W.; Ghorannevis, Z.; Amara, K. K.; Pang, J. R.; Toh, M.; Zhang, X.; Kloc, C.; Tan, P. H.; Eda, G. Lattice Dynamics in Mono- and Few-Layer Sheets of WS_2 and WSe_2. *Nanoscale* **2013**, *5*, 9677–9683.
25. Mooradian, A.; Wright, G. B.; Cooper, W. C. *The Physics of Selenium and Tellurium*; Pergamon Press: Oxford, U.K., 1969; p 269.
26. Masuzawa, T.; Saito, I.; Yamada, T.; Onishi, M.; Yamaguchi, H.; Suzuki, Y.; Oonuki, K.; Kato, N.; Ogawa, S.; Takakuwa, Y.; *et al.* Development of an Amorphous Selenium-Based Photodetector Driven by a Diamond Cold Cathode. *Sensors* **2013**, *13*, 13744–13778.
27. Shpak, A. P.; Korduban, A. M.; Medvedskij, M. M.; Kandyba, V. O. XPS Studies of Active Elements Surface of Gas Sensors Based on WO_{3-x} Nanoparticles. *J. Electron Spectrosc. Relat. Phenom.* **2007**, *156*−*158*, 172–175.
28. Boscher, N. D.; Carmalt, C. J.; Parkin, I. P. Atmospheric Pressure Chemical Vapor Deposition of WSe_2 Thin Films on Glass-Highly Hydrophobic Sticky Surfaces. *J. Mater. Chem.* **2006**, *16*, 122–127.
29. Salitra, G.; Hodes, G.; Klein, E.; Tenne, R. Highly Oriented WSe_2 Thin Films Prepared by Selenization of Evaporated WO_3. *Thin Solid Films* **1994**, *245*, 180–185.
30. Lim, B. S.; Rahtu, A.; Gordon, R. G. Atomic Layer Deposition of Transition Metals. *Nat. Mater.* **2003**, *2*, 749–754.
31. Panish, M. B. Molecular Beam Epitaxy. *Science* **1980**, *208*, 916–922.
32. Vispute, R. D.; Talyansky, V.; Trajanovic, Z.; Choopun, S.; Downes, M.; Sharma, R. P.; Venkatesan, T.; Woods, M. C.; Lareau, R. T.; Jones, K. A.; *et al.* High Quality Crystalline ZnO Buffer Layers on Sapphire (001) by Pulsed Laser Deposition for III-V Nitrides. *Appl. Phys. Lett.* **1997**, *70*, 2735–2737.
33. Lee, L. T. L.; He, J.; Wang, B.; Ma, Y.; Wong, K. Y.; Li, Q.; Xiao, X.; Chen, T. Few-Layer $MoSe_2$ Possessing High Catalytic Activity towards Iodide/Tri-iodide Redox Shuttles. *Sci. Rep.* **2014**, 4.
34. Tsirlina, T.; Feldman, Y.; Homyonfer, M.; Sloan, J.; Hutchison, J. L.; Tenne, R. Synthesis and Characterization of Inorganic Fullerene-like WSe_2 Materials. *Fullerene Sci. Technol.* **1998**, *6*, 157–165.